Optical and Quantum Electronics (2022) 54: 635
https://doi.org/10.1007/s11082-022-03994-0

Theoretical and experimental investigation of the electronic and optical properties of pure and interstitial nitrogen -doped $(TiO_2)_n$ cluster

Shaida Anwer Kakil[1] · Hewa Y. Abdullah[2] · Tahseen G. Abdullah[1]

Received: 10 October 2021 / Accepted: 12 July 2022 / Published online: 24 August 2022

Abstract
The structural and electronic properties of pure and nitrogen-doped TiO_2 nanoclusters are investigated using density functional theory with vibrational modes. We performed numerical simulation using two methods based on theories at the Quantum Espresso/PBE and Gaussian/B3LYP/631G (d) levels. The properties of a single nitrogen-doped $(TiO_2)_n$ nanocluster are also computed in this study. In both cases, interstitial and substitutional Nitrogen doping at all accessible sites was examined. For the experiment, Supersonic Cluster Beam Deposition (SCBD) was used to create pure and nitrogen-doped TiO_2 films of nanocluster assemblies. Atomic force microscopy, X-ray photoelectron spectroscopy (XPS), UV–Vis spectroscopy, and Raman techniques were used to characterize these samples. The binding energies (Np, O2s, Ti 2p1/2, and Ti 2p3/2) of N-doped TiO_2 were estimated using XPS spectral results. The UV–Vis measurement confirmed the previously stated reasoning about the quantum size effect on the band gap of the pure and nitrogen doped TiO_2 nanocluster. The theoretical vibrational modes frequencies are calculated using the B3LYP/6-31G (d) functional via the Gaussian16 code's implementation algorithm. The good agreement between simulation and experimental results implies that a significant advantage of interstitial over substitutional positions. N–O vibration modes appeared in interstitial doped TiO_2, and each vibration was dependent on a different cluster structure.

Keywords N doping · $(TiO_2)_n$ nanocluster · Interstitial · DFT · Vibrational mode

1 Introduction

Nitrogen doped titanium dioxide is gaining popularity due to its potential as a material for environmental photo catalysis. In the last year, numerous theoretical and experimental studies on doped TiO_2 have been published. Controlling the size of the nanostructure, on

✉ Shaida Anwer Kakil
Shaida.Kakil@su.edu.krd

[1] Department of Physics, College of Science Salahaddin University, 44001 Erbil, Iraq

[2] Physics Education Department, Faculty of Education, Tishk International University, 44001 Erbil-Kurdistan Region, Iraq

the other hand, is both a problem and a pipe dream for many researchers. The following papers, published in recent years, investigate the physical and chemical properties of TiO_2 nanoclusters experimentally and theoretically. I. Shyjumon et al. (2006) created titanium clusters on a silicon substrate using magnetron sputtering, followed by aggregation in an argon gas flow. Clusters typically range in size from 8 to 13 nm. Drabik et al. (2011) investigated the design and fabrication of titanium nanocluster films using a magnetron-sputtering gas-aggregation cluster source. Srivastava et al. (2014) successfully manufactured and collected size-selected TiO_2 nanoclusters at room temperature on three distinct substrates: Si, glass, and quartz. They used a special magnetron-sputtering source followed by a quadrupole mass filter. Transmission electron microscopy revealed that NCs larger than a primary size (eight nanometers) have a translucent center with a shapeless shell. Chiodi et al. (2012) used Supersonic Cluster Beam Deposition (SCBD) to create co-doped Cr–N TiO_2 films with significantly improved absorbance in the visible and near infrared. The Cr and N dopants are involved in substitution sites. According to the spectroscopic data, the general impact of N and Cr substitution co-doping results in the presence of new electronic states at the highest point of the Valence band (VB). Many researchers have reported TiO_2 clusters in theory: DFT was used by Arab et al., (2016) to investigate the electronic structure and reactivity of $(TiO_2)_n$ ($n = 1$–10) nano-clusters. The binding energy per atom, second-order energy difference, and fragmentation energy were all used to discuss cluster stability.

Fronzi et al. (2016) demonstrated the effect of TiO_2 nanocluster alteration providing valuable guidelines for further developing TiO_2 photo catalytic (UV and visible light) movement, which will be useful for oxidative degradation of organic pollutants or CO_2 reduction by utilizing combined DFT recreation and experimentation. The optical absorption spectra of $(TiO_2)_n$ ($n = 1$–20) nanoclusters and ($n = 35$, 84) nanoparticles have been computationally investigated in gas phase and in water as solvent by Valero et al. (2018) based on the analysis of the frequency-dependent dielectric function in the independent particle approximation within the framework of the density functional theory. Villanueva et al. (2015) used DFT to investigate the underlying and electronic properties of Ti_9XO_{20} (X = Ti, C, Si, Ge, Sn, and Pb) clusters in order to provide an alternative to experimental strategies for developing new materials with high synergist applications. Kroes and Qu et al.(2006) investigated the electronic structure and steadiness of both nonpartisan and independently charged $(TiO_2)_n$ groups with $n = 19$ using the DFT with B3LYP/LANL2DZ strategy. The steady construction of TiO_2 nanoclusters resulted in a general frame with a minimal design and a couple of Ti–O terminal bonds. A few researchers have also theoretically and experimentally focused on the band gap of TiO_2 as a function of particle size. Monticone et al. (2000). investigated the TiO_2 anatase crystalline phase and discovered that the band gap energy did not vary with size down to 2R = 1.5 nm. According to UV–vis absorbance measurements, Lin et al. (2006) believe there is no variation in band gap energy with size. Besides that, they used the MOCVD method to create TiO_2 crystalline with varying particle sizes (particle size ranged between 12 and 29 nm). The band gap of TiO_2 nanoparticles varies with primary particle size. Karkare (2014) proved that the band gap increased with particle size. With decreasing particle size, the absorption edge shifted to higher energy (blue shift). They demonstrated that a smaller crystallite size (8.4–10.6 nm) should have a larger band gap of 3.4 eV. Mandal et al. (2019) investigated the optical band gap of these nano composites for pure TiO_2, using 3.7 eV as a reference.

In this study, Ab initio calculations are performed and electronic properties for pure N-doped TiO_2 are investigated in order to assess the change in properties with respect to the N content. The formation energies of pure and N-doped TiO_2 were computed using two different DFT models: Quantum Espresso/PBE and Gaussian/B3LYP/6-31G (d). The

results were analyzed and compared to the experimental. Experimental we report the morphological and structural characterization of nanostructured TiO_2 nano produced by supersonic cluster beam deposition (SCBD).

2 Material and method

2.1 Experimental: synthesis of nitrogen-Doped TiO_2 cluster

Supersonic cluster beam deposition (SCBD) was employed to prepare pure and nitrogen-doped TiO_2 nanostructured films on silicon and quartz substrates, using a Pulsed Micro-Plasma Cluster Source (PMCS) from LGM/CIMaINa A detailed description of the Supersonic cluster beam deposition can be found in references (Barborini et al. 1999; Milani et al. 2001; Piseri et al. 1998): a pulsed electric-discharge between the target-material (Ti) - as the cathode - and a second electrode – as the anode - vaporizes the target via sputtering ablation. The discharge is confined to a micro-plasma region at the cathode surface through controlled injection of a process gas (inert: typically He or Ar for metallic clusters, or an oxygen-containing mixture for oxide nanoparticles) with a pulsed solenoid valve. precise control of the gas mixture allows fine tuning on the composition of the nanoparticles that are formed upon condensation of the vapor: for N-doped TiO_2, 99.80% (Ar), 0.015% (O_2), and 0.05% (N_2) were used. The thus-formed nanoparticles suspension is evacuated from the PMCS via a nozzle, generating a seeded supersonic beam of nanoparticles that can be deposited on any substrate intercepting the beam along the propagation direction. The surface morphology of the samples was investigated using AFM (Stylus profilometer KLA Tencor P6). The optical band gap of a pure cluster- TiO_2 and for N-doped TiO_2 were determined using UV–vis spectroscopy (Agilent Cary 100 UV–Vis spectrophotometer) in the wavelength range of 100–800 nm. Surface chemical compositions and chemical status were analyzed by using XPS (Leybold LHS 10/12). Raman spectra of the cluster pure and Nitrogen doped TiO_2 on silicon were recorded by Raman spectroscopy in CIMaINa, an assembled spectroscopic system consisting in an Ar ion laser emitting at 514 nm (Spectra Physics, beamlok series 2065–7) as the excitation source. A single monochromator (Acton SP-2558-9 N) equipped with a 1200 blaze mm-1 grating, a notch filter (Razoredge long wave pass filter), and a liquid nitrogen-cooled CCD camera (Roper-Princeton Instruments SPEC10:400B/LN).

2.2 Theoretical: computational methods (DFT)

To obtain the optimized structure, the configuration is geometrically fully relaxed using the DFT model. To compute the electronic and vibrational properties of pure and N-doped TiO_2, we used quantum chemical calculations DFT (Gaussian 16 program package) and Quantum ESPRESSO. The PBE functional(Giannozzi et al. 2009), ultra soft Vanderbilt pseudopotentials(Kresse and Joubert 1999), and a plane-wave (PWs) basis set with a cut off of charge density (30 Ry and 300 Ry) were used to perform structural relaxations with the code Quantum ESPRESSO simulation package. We used Gaussian 16 (Frisch et al. 2016) with hybrid B3LYP(Lee et al. 1988) functional basis sets 6-31G(d) to compute the electric and vibrational modes other than plane waves (PWs). Figure 1 depicts an optimized structure of $(TiO_2)_n$:Ti_9O_{18} and $Ti_{28}O_{56}$. It was chosen from among the structures

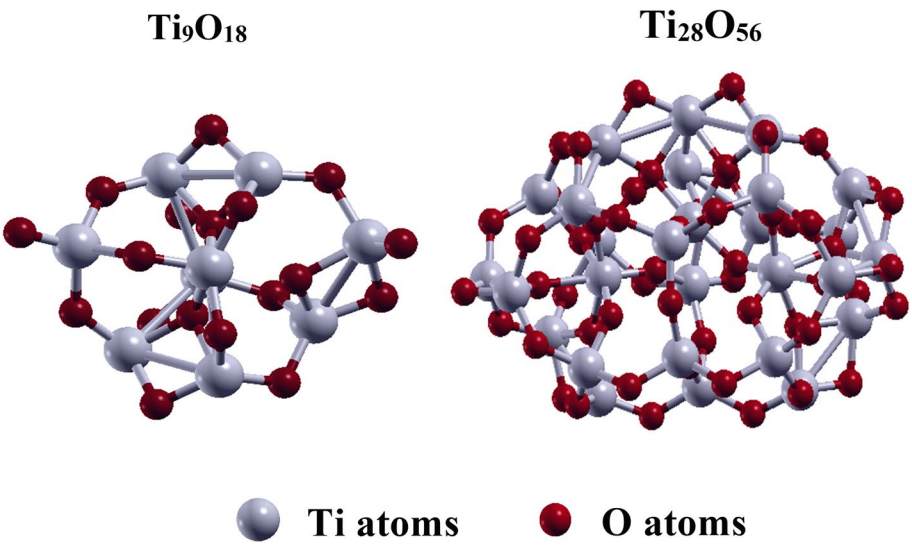

Fig. 1 DFT Optimized structure of different nanocluster: Ti_9O_{18} and $Ti_{28}O_{56}$ by using DFT/Quantum ESPRESSO

determined by global optimization using interatomic potentials in recent works(Lamiel-Garcia et al. 2017).

3 Results and discussions

3.1 Bond lengths and formation energies: substitutional and interstitial case of ($Ti_{28}O_{55}N_1$) and TiO_2 ($Ti_{28}O_{56}N_1$) cluster in different configuration

When the nitrogen substituents incorporate into the TiO_2, the formation energy altered function of impurity position and Ti–N bond lengths are of course altered compared to the pristine Ti–O bonds. Several additional publications have noted the effect of impurity location on TiO_2 electronic characteristics. Giovanni Di Liberto et al. (2019) investigated nitrogen doping that is exposed to (001)–(101) Anatase TiO_2 Surfaces and discovered that N001 is the most stable doping arrangement, with the nitrogen atom on the (001) side of the interface. kakil et al. (Kakil et al. 2020) demonstrated that nitrogen doping in TiO_2 anatase is subsurface depth dependent in substitution and interstitial doped forms, and that nitrogen impurity locations are dependent on nanocrystal facet (Kakil et al. 2021). They also investigated the formation of nitrogen impurity in TiO_2 nanoparticles and how the mid-gap state of TiO_2 nanocrystal is generated, as well as how the nitrogen impurity locations depend on facet of nanocrystal.

Figure 2 shows the optimal structure of $Ti_{28}O_{55}N_1$ obtained by inserting one substitution N atom in an O lattice location in various configurations using DFT/PBE. Each number in Table 1 corresponds to the formation energies of nitrogen doped TiO_2 ($Ti_{28}O_{55}N_1$) at various sites. Ns-Cl.n Ns is for Nitrogen substitution doped, and Cl.n stands for impurity at various positions in the cluster, with n ranging from 1 to 9, corresponding to each location

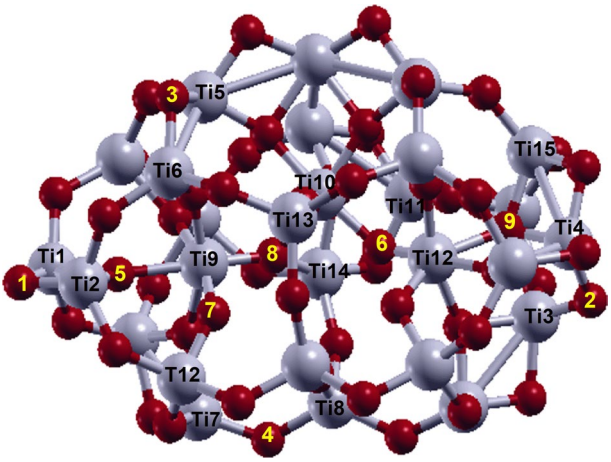

Fig. 2 Labeling of Nitrogen substitutional positions for ($Ti_{28}O_{55}N_1$) cluster

Table 1 Formation energy (E_f) and the defect gap (E_{IL}-$E_{V\,B}$) of substitutional-N-doped ($Ti_{28}O_{55}N_1$) nanocluster at a different position

$Ti_{28}O_{55}N_1$	E_f [eV]	$E_{IL} - E_{V\,B}$[eV]
Ns-Cl.1	5.321	1.0456
Ns-Cl.2	5.152	0.977
Ns-Cl.3	5.125	0.696
Ns-Cl.4	5.070	1.041
Ns-Cl.5	5.080	1.326
Ns-Cl.6	5.018	1.259
Ns-Cl.7	5.052	0.965
Ns-Cl.8	4.869	1.270
Ns-Cl.9	4.685	1.314

in Fig. 2. Equation 1 was used to calculate the formation energies of nitrogen substitution sites.

$$E_f = E_{1N\,nanocluster} - E_{nanocluster} + \frac{1}{2}E_{O_2} - \frac{1}{2}E_{N_2} \tag{1}$$

Table 1 shows the formation energy and defect gap of a substitution-N-doped ($Ti_{28}O_{55}N_1$) nanocluster at various positions. The formation energy varied from 5.321–4.685 eV, whereas the defect energy varied from 1.314 to 0.696 eV. As seen in (Ns-Cl6, Ns-Cl7, Ns-Cl8, and Ns-Cl9), the nitrogen atom inside the cluster has lower formation energy than the nitrogen atom outside the cluster (Fig. 3). The formation energy of cluster Ns-Cl9 is 4.685, which is lower than the formation energy of another cluster impurity position. The electronic structure of a cluster is affected by the location of nitrogen impurities. According to Table 1, the energy differences are around 0.625 eV, although in the case of clusters, the majority of atoms are at the surface and Atom clusters have considerably different physical and chemical properties than bulk solids of the same composition. The discrepancy arises from the fact that a high proportion of their component atoms are situated at the surface. Figure 4 depicts the influence of impurity position on bond-length change of various substitution positions of nitrogen dopants in the ($Ti_{28}O_{55}N1$) cluster.

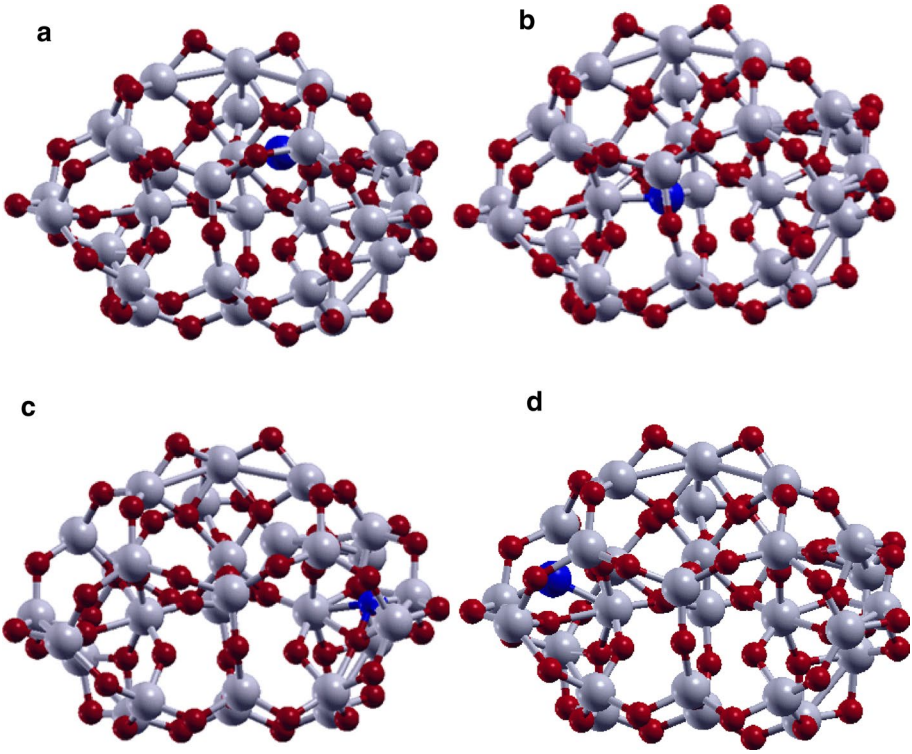

Fig. 3 Optimized structure nitrogen atom at a different position for ($Ti_{28}O_{56}N_1$) cluster interstitial case, The gray (light) red (dark), blue balls correspond to Ti O and N, respectively. (Color figure online)

We doped TiO_2 in four distinct sites for nitrogen to explore interstitial N doping, as illustrated in Fig. 3. Equation 2 is used to compute the formation energy.

$$E_f = E_{1Nnanocluster} - E_{nanocluster} - \frac{1}{2}E_{N_1} \tag{2}$$

The formation energy, defect gap, and N–O bond length of interstitial -N-doped ($Ti_{28}O_{56}N_1$) clusters at different positions are shown in Table 2. The influence of impurity position on defect gap and the N–O bond produced in the case of interstitial have different lengths depending on impurity position. Because of the low formation energy, interstitial is more beneficial than substitution in terms of impurity position. We studied (Ni-Cl.4) for the electronic structure investigation because it has a lower formation.

3.2 Electronic properties of pure $Ti_{28}O_{56}$ and nitrogen doped ($Ti_{28}O_{56}N_1$)

The density of State (DOS) was computed using Gaussian16 software to investigate the electrical characteristics of the examined structures. Any material's electronic density of states provides enough information to comprehend its electronic characteristics fully. A density-of-state (DOS) diagram can be used to visualize the energy level distribution (Gui et al. 2019). TiO_2 and N-doped TiO_2,nanocluster wave function was calculated using Density Functional Theory (DFT), B3LYP at 6-31G(d) basis set. Figure 5 compares the density

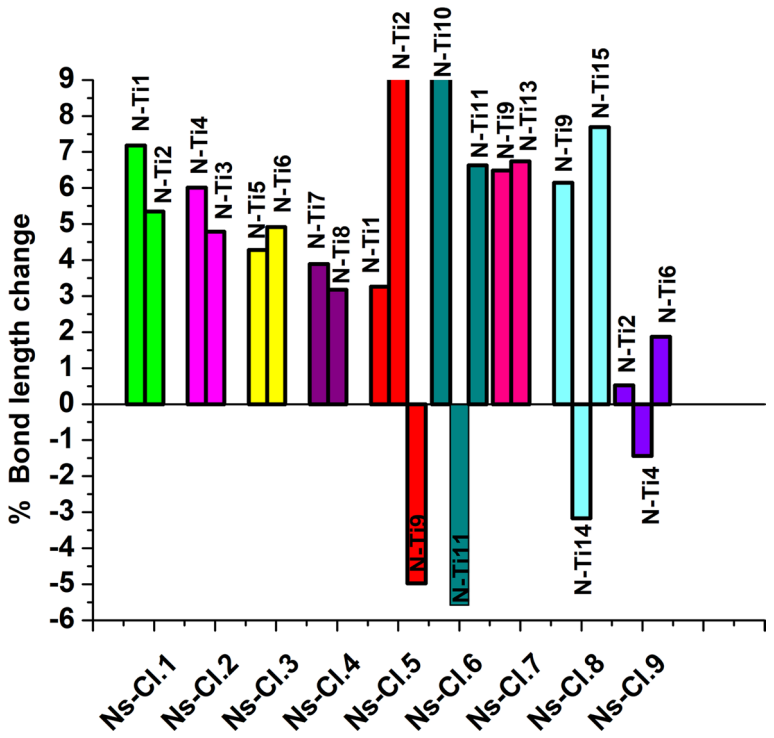

Fig. 4 The percent fraction bond lengths of different substitutional positions of nitrogen dopants in titanium oxide ($Ti_{28}O_{55}N_1$) cluster. The bonds length around the N atom is identified in Fig. 2

Table 2 Formation energy (E_f), the defect gap (E_{IL}-$E_{V\,B}$), and N–O bond length of interstitial -N-doped ($Ti_{28}O_{56}N_1$) cluster at a different position

$Ti_{28}O_{56}N_1$	E_f [eV]	E_{IL}-$E_{V\,B}$[eV]	N–O[pm]
Ni–Cl.1	3.910	1.617	137
Ni–Cl.2	3.820	0.914	133
Ni–Cr.3	3.527	1.291	135
Ni–Cl.4	2.9	1.253	134

of states (DOS) for pure ($Ti_{28}O_{56}$) and nitrogen doped ($Ti_{28}O_{55}N_1$) Nano clusters. Significant impurity states are introduced into the gap as a result of doping. Following the addition of one nitrogen, the states emerge at the top of the conduction band. N's action defines the creation of the ionic N–O bond as a p dopant. N (p) helps to narrow the gap by producing the valence and conduction bands.

After the Nitrogen atom was inserted into the TiO_2 structure, the HUMO-LUMO gap was reduced from 3.772 to 2.389 eV. A significant change can be seen in these graphs. UV absorption spectra, which will be examined in the next section, revealed this behavior. Because the band gap of the Quantum Espresso/PBE-GGA method was underestimated, we employed the Gaussian/B3LYP approach. The gap energy reduces from 2.826 to 1.257 eV calculated by Quantum Espresso/PBE-GGA, as shown in Table 3. The electronic band and defect band in [eV] for pure $Ti_{28}O_{56}$ and nitrogen doped TiO_2 ($Ti_{28}O_{56}N_1$) were calculated

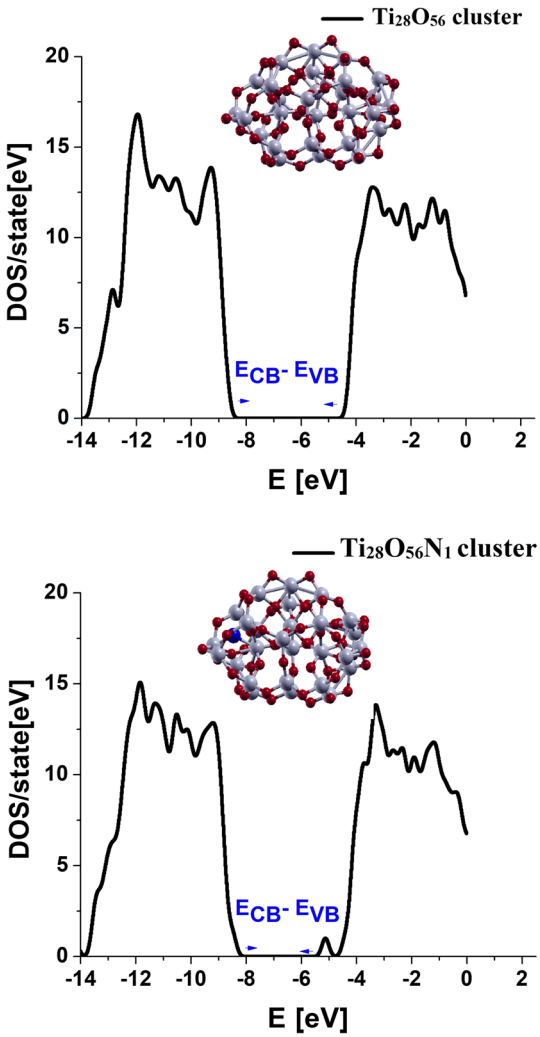

Fig. 5 Density of state diagrams for (DOS) for pure ($Ti_{28}O_{56}$) and Nitrogen doped ($Ti_{28}O_{56}N_1$). Data were obtained from B3LYP/6-31G(d)

using both Quantum Espresso/PBE-GGA and Gaussian/B3LYP/6-31G(d) approaches, and the results were compared to previous literature(Cao et al. 2021; Lundqvist et al. 2006; Oprea and Gîrțu 2019; Persson et al. 2000; Selli et al. 2017).

3.3 Surface morphology of N-doped TiO_2 nanocluster

Atomic force microscopy AFM was used to analyze the surface morphology of nanostructured Nitrogen-doped TiO_2. Figure 6 shows the surface morphology of the N doped TiO_2 cluster layer formed on silicon and a histogram of particle size distribution. As seen in the histogram, the clusters appear to be almost spherical, with an average lateral size of less than (2 nm) and some of them having an average size of 5 nm.

Table 3 The Band gap and defect gap in unit [eV] for pure $Ti_{28}O_{56}$ and nitrogen doped TiO_2 ($Ti_{28}O_{56}N_1$) utilizing Q.E espresso/PBE-GGA and Gaussian/B3LYP/6-31G (d) methods

Cluster	Method	Band gap [eV]	Defect band gap[eV]
$Ti_{28}O_{56}$	PBE	2.826 [this work]	1.257
$Ti_{28}O_{56}$	B3LYP/6-31G(d)	3.772 [this work]	2.893
$Ti_{28}O_{56}$	B3LYP/VDZ//PW/SZ	3.67 Mahmoud et al. (2021)	
$(TiO_2)_{101}$·6H2O	DFT(B3LYP)	3.81 Majid and Bibi (2017)	
$Ti_{24}O_{50}H$	B3LYP/LANL2DZ	3.8 Mandal et al. (2019)	
$(TiO_2)_{101}$·6H2O	DFTB	3.2 Majid and Bibi (2017)	
$Ti_{29}O_{58}$	Gaussian03/B3LYP/6311G	3.33 Milani et al. (2001)	
$Ti_{38}O_{76}$	INDO/S-CI	3.5 Manticone et al. (2000)	

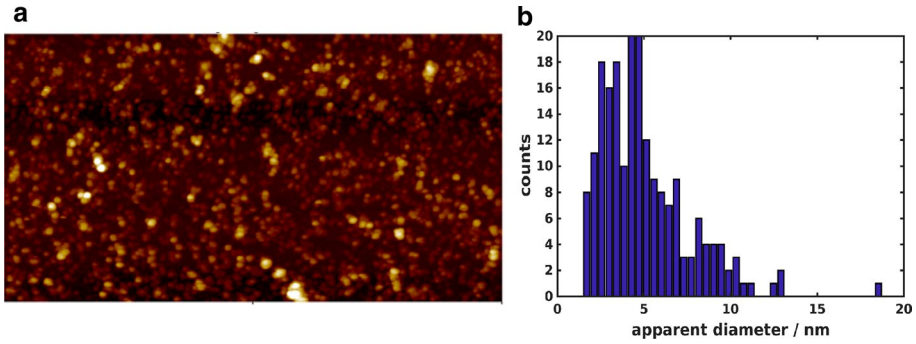

Fig. 6 **a** AFM image of the surface morphology of N doped TiO_2 cluster film deposited on silicon, **b** Histogram of particle size distribution

The smallest visible grains (2 nm) are primeval clusters created in the source, while larger grains produce smaller clusters aggregating and coalescing.

3.4 X-ray photoelectron spectroscopy (XPS)

XPS analysis was used to analyze the chemical composition and chemical state of the TiO_2 nanoclusters. Figure 7 shows the XPS spectra of N-doped TiO_2, where the peaks at 401.7, 459, 464, and 530.17 eV correspond to the binding energy of N1s, $Ti2P_{1/2}$, $Ti2P_{3/2,}$ and O 1s peaks. The N1s reveal the presence of nitrogen in the nanostructured material (inset Fig. 7). The peaks are in the range (396–404 eV) seen by numerous other writers, although Di Valentin et al. (2007) detected a peak at higher binding energy (400 eV). This peak at this energy represents the interstitial-site nitrogen (Ti–O–N) in which the N atoms are bound to lattice oxygen atoms. This peak at this energy represents the interstitial-site nitrogen.

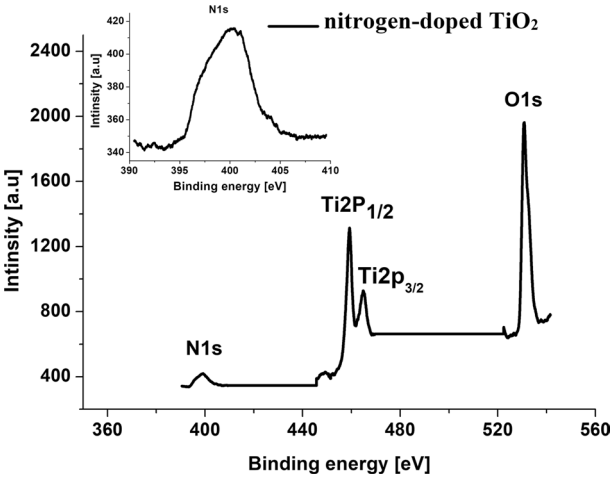

Fig. 7 XPS of Nitrogen doped TiO_2 as generated, inset Fig. N1s peak centered at 400 eV for N-TiO_2

3.5 Optical properties of the pure and nitrogen-doped TiO_2

A UV- visible absorption spectrum was performed to analyze the optical absorbance of pure and nitrogen-doped TiO_2 nanoclusters. If the semiconductor size is smaller than the Bohr radius of the excited state, the quantum confinement effect is expected, and the absorption edge will be shifted to higher energy. More study is being done on the quantum confinement effect of TiO_2 as well as direct and indirect band gaps. Yin Zhao and Chunzhong Li et al. (2007)found that the band gap of as-prepared TiO_2 nanoparticles is 3.28 eV, which is somewhat higher than the value of 3.2 eV for bulk TiO_2 due to the quantum size impact of the present TiO_2. In anatase TiO_2 nanoparticles, Madhusudan Reddy et al. (2003) indicated that the direct, rather than indirect, transition is more beneficial, as shown in Table 4. Figure 8 shows the UV–vis spectra of pure and Nitrogen-doped (TiO_2) nanostructures. The plots of $(\alpha.h\nu)^2$ vs the energy level of the absorbed light are shown in the inset Fig. 8. The Wood and Tauc equation, which is defined as follows, is used to estimate the band gap value.

Table 4 Experimental band gap in unit [eV] for pure and nitrogen-doped TiO_2 compared with previous works

Nano composites	Size [nm]	Bandgap [eV]	References
TiO_2 nanocluster	2–5	3.75	This work
N-TiO_2 nanocluster	2–5	3.56	This work
Quantum dot	5	~3.76	Qu and Kroes (2006)
Quantum dot	3–7	3.79	Salazar-Villanueva et al. (2015)
Nanoparticle	11	3.4	Giannozzi et al. (2009)
Nanoparticle	10	3.35	Persson et al. (2000)
N-doped nanoparticle	10	3.05	
Nanoparticle	20	3.75	Gnanasekaran et al. (2015)

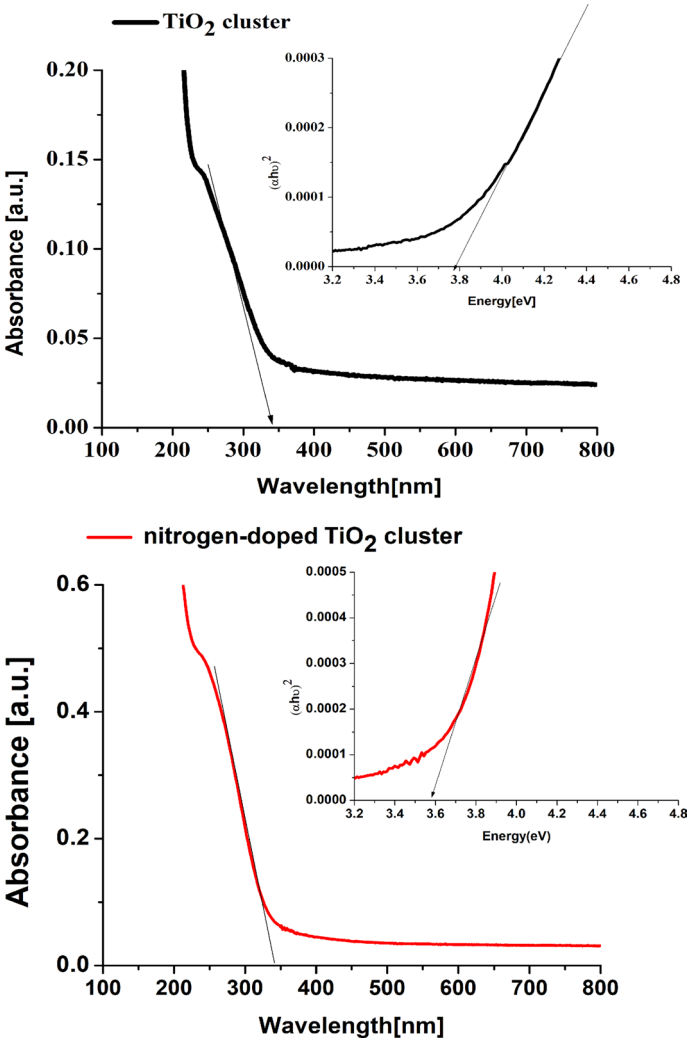

Fig. 8 UV–vis spectra of pure and Nitrogen-doped (TiO_2) nanostructure inset Fig. represents the plots of $(\alpha.h\nu)^2$ versus the energy level of the absorbed light

$$\alpha h\upsilon = \mathrm{K}\left(h\upsilon - \mathrm{E_g}\right)^{\mathrm{n}} \tag{3}$$

where K, hν, and Eg are constant, photon energy, and optical band gap, respectively. n is equal to 1/2 for allowed direct optical transitions, and α is the absorption coefficient. The band gap values were determined by extrapolating the linear region of the plot to $h\nu = 0$. From the Tauc plots of $(\alpha h\nu)^2$ versus hν. The direct band gap of TiO_2 nanopartical observed (Jia et al. 2018; Karkare 2014; Mahmoud et al. 2021; Mandal et al. 2019) With the addition of nitrogen atom, the band gap decreased from 3.75 to 3.560 eV, and the results were summarized in Table 4. It displays the experimental measurements of band gap in [eV] units and compares them with previous works (Gnanasekaran et al. 2015; Javed et al. 2019; Jia

et al. 2018; Karkare 2014; Mandal et al. 2019). Because its p states contribute to band gap narrowing by mixing with O 2p and N (p) states, the N atom's lowered band gap was the most effective. The excitation wavelengths were found by DFT (B3LYP/6-31G(d)) for pure and nitrogen-doped TiO_2 (350.96 and 411.00 nm), respectively.

3.6 Experimental and theoretical DFT-B3LYP/6-31G (d) investigation of Raman spectra for pure and nitrogen doped TiO_2

3.6.1 Raman analysis

The following representation for optical vibrational modes at the Γ point of bulk TiO_2 was derived from a group theoretical analysis:

$$A_{1g} + 1\ A_{2u} + 2\ B_{1g} + 1\ B_{2u} + 3\ E_g + 2\ E_u$$

It consists of three Raman active modes ($A_{1g}+1\ B_{1g}+3\ E_g$), two modes are infrared active ($1\ A_{2u}+2\ E_u$), and one mode ($1\ B_{2u}$) is inactive in both Raman and infrared(Ohsaka 1980). The vibration mode of TiO_2 was impacted by size, annealing, architectures, and other factors; Xu et al. (2001) explained the variation in the Raman bands with a phonon confinement model based on the Heisenberg uncertainty principle. They showed that the phonon becomes increasingly confined within the particle and the phonon momentum distribution as particle size decreases.

Flavio Della Foglia et al. (2009) synthesized the TiO_2 nanostructured film via (SCBD). Raman spectroscopy indicated no crystalline structure after annealing at 200 °C, indicating that the film is predominantly amorphous. They also demonstrated that the shape of nanostructured TiO_2 films could improve annealing for photocatalytic applications. Hengzhong Zhang (2008) reported a combination of experimental and computational modeling to investigate amorphous titanium made up of 2 nm TiO_2 nanoparticles. The nanoparticles contain a severely deformed shell and a stretched anatase-like core, according to the researchers. The weak Raman scattering in these films is attributed to the low phonon density of states in the amorphous phase, as seen in Fig. 9, which exhibits Raman spectra of pure and Nitrogen-doped

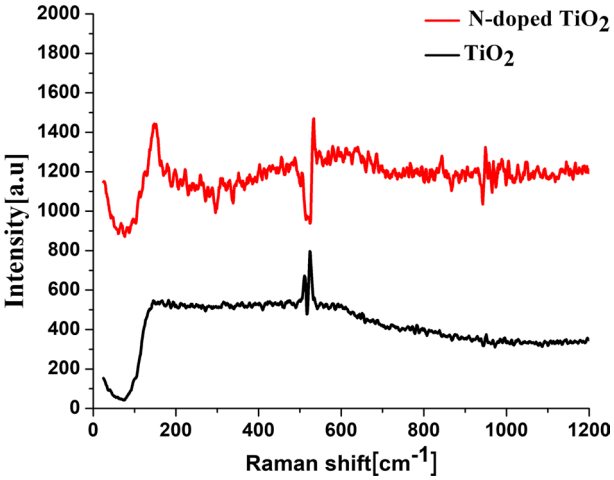

Fig. 9 Raman spectra of pure and Nitrogen-doped (TiO_2) nanocluster

TiO_2 clusters without annealing. The no observed Raman bands in an amorphous solid are no longer related to traveling waves or wave vectors, as are no longer phonons.

3.6.2 Theoretical vibrational properties of pure and N-doped (TiO2)n by DFT/B3LYP/6-31G(d)

Ogata et al. (1999) employed modified variable charge interatomic potential to examine the structural and physical features of nano size TiO_2 clusters of 1050 and 672 atoms at 100 K using molecular dynamics (MD) simulations. We reveal the Ti–O bonding characteristics that play a key role in replicating macroscopic and microscopic values with accuracy comparable to that of first-principles computations. Kulbir Kaur Ghuman et al. (2013) investigated the vibrational characteristics of rutile supercells and rutile and amorphous TiO_2 nanoparticles using the Matsui and Akaogi rigid ion model with effective charges on Ti and O atoms. They demonstrated that the phonon bandwidth and dispersive character of optical phonon modes in higher frequency ranges agree with experimental results. However, the calculated and experimental findings are within 15% of each other in the intermediate energy range, while the calculated results are higher than the experimental values in the lower energy range.

In a $(TiO_2)_n$ cluster, if n changes, the majority of physical properties change as well. The clusters were constructed by Brandon Bukowski et al. (2015) with $n=1$, 3, 5, 8, and 15 total atoms, or 3, 9, 15, 24, and 45 total atoms, respectively. For each cluster size, there are a number of possible structural isomers. When a result, as cluster sizes get larger, atoms tend to adopt higher coordination, eventually embracing bulk coordination with the correct cluster size.

The vibrational modes of $Ti_9O_{18}$and $Ti_{28}O_{56}$ clusters were calculated in this study. Except for Ti_2O_4 spectral investigation (Majid and Bibi 2017), none of the above physical attributes have been explored by any other researcher.

Because there are multiple coordinates of Ti (1Ti, 2Ti, 3Ti…) for any given cluster size, we have 74 modes of vibration in Ti_9O_{18} clusters, the majority of which are different from Ti_2O_4 due to different structures. As cluster sizes rise, the atoms tend to adopt higher coordination, as shown in Fig. 10, which shows the Raman activity spectra of Ti_9O_{18} and Ti_28O_{56} computed using Gaussian/B3LYP 6-31G (d), with two strong peaks appearing about 1040.92 cm^{-1} and 1045.45 cm^{-1}. These two vibrations do not exist in the cluster ($Ti_{28}O_{56}$) because both cluster sides have 1Ti coordinates, as shown in Fig. 11. The arrow represents the O-1Ti vibration mode. We believe all clusters cannot have the same vibration, which is dependent on cluster structure. The Raman spectrum activity of pure ($Ti_{28}O_{56}$) and nitrogen doped ($Ti_{28}O_{56}N_1$) Nano clusters are displayed in Fig. 12 using Gaussian/B3LYP/6-31G (d). The (*) peak of pure Ti–O demonstrates the stretched bonds ($Ti_{28}O_{56}$). The vibrational mode N–O of nitrogen doped ($Ti^{28}O5^6N^1$) at approximately 1013.9 cm^{-1} is depicted in the inset Fig. 12. This is a stretching mode that has been investigated in N-doped TiO_2.

4 Conclusions

The following goals are pursued using experimental and theoretical studies (DFT/B3LYP/6-31G (d) techniques and the Quantum espresso code).

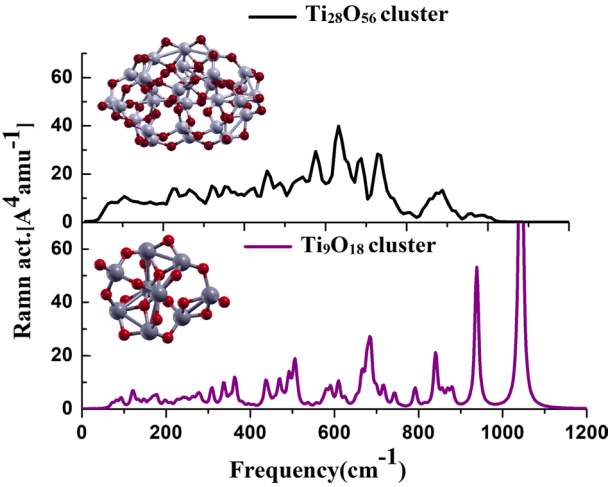

Fig. 10 Raman activity of Ti_9O_{18}, and $Ti_{28}O_{56}$ calculated using Gaussian/B3LYP/6-31G(d)

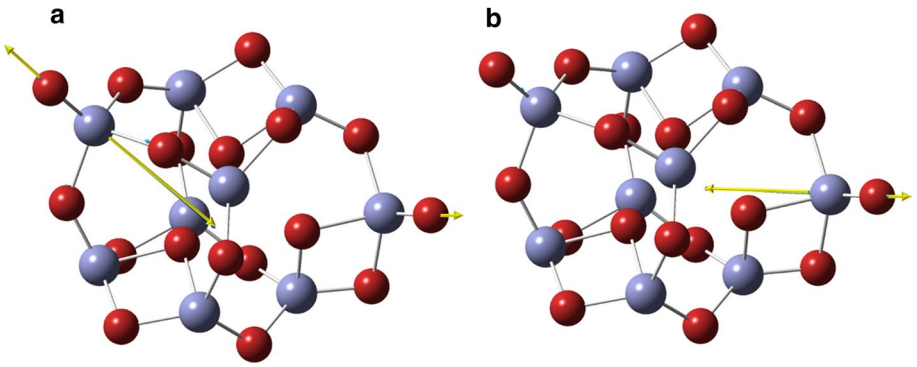

Fig. 11 Mode of vibration (Ti_9O_{18}) at 1040.92 $cm^{-1}$and 1045.45 cm^{-1} by Gaussian/B3LYP/6-31G(d). The gray (light) and red (dark) balls correspond to Ti and O, respectively. (Color figure online)

(i) Structural and Electronic characteristics of pure and nitrogen doped $(TiO_2)_n$ clusters were examined using two DFT level theories: Quantum Espresso/PBE and Gaussian/B3LYP/6-31G (d).

(ii) The synthesis of TiO_2 and nitrogen doped TiO_2 nanoclusters was achieved using Supersonic Cluster Beam Deposition (SCBD). The size of the particles is estimated to be in the range of (2–5 nm).

(iii) We discovered the effect of impurity position on formation energy and electronic characteristics in both interstitial and substitution cases in an optimized structure. We assumed that doped nitrogen in TiO_2 clusters is positioned at the interstitial site of the TiO_2 lattice based on formation energy, which is compatible with XPS data (O–Ti–N).

(iv) The band gap energy dropped for the N-doped TiO_2 clusters, according to UV–Vis spectroscopy. As a result of the theoretical conclusions, the band gap is predicted to decrease when N is doped.

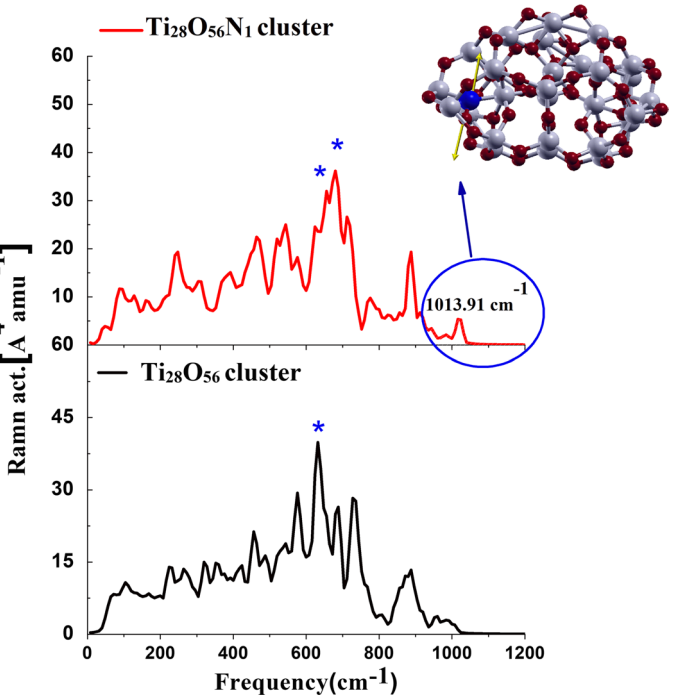

Fig. 12 Raman spectral activities for pure ($Ti_{28}O_{56}$) and Nitrogen-doped ($Ti_{28}O_{56}N_1$) nanoclusters using Gaussian/B3LYP6/31G (d). The inset Fig. represents the vibrational mode of N–O. The gray (light), red (dark), and blue balls correspond to Ti, O, and N. (Color figure online)

(v) The addition of N as a dopant result in forming a new N–O band with the vibration of (1013.91 cm^{-1}) at Gaussian/B3LYP/6-31G (d), implying the emergence of states in band states with a narrowing of the bandgap.

(vi) The quantum confinement effect was observed using UV- Vis Spectroscopy, with a significant band gap energy of pure TiO_2 (3.753 eV) and the theoretical band gap (3.772 eV) via DFT/B3LYP/6-31G (d) basis set.

(vii) Raman spectral activity of Ti_9O_{18} and $Ti_{28}O_{56}$ nano clusters has been studied using Gaussian/B3LYP/6-31G (d) basis set.

(viii) We believe this research is important because it has the potential to aid in the study and characterization of the physics and materials science of TiO_2. This material that has received a lot of attention in recent years. Due to its significance for titanium nanocluster, it may also have an impact on nanoscience.

Acknowledgements The authors would like to thank Nicola Manini from Universita degli Studi di Milano-Italy for providing computational facilities and outstanding scientific advice. Special thanks to Alessandro Podestà and Paolo Piseri from CIMaIna laboratories at Università degli Studi di Milano (Milano, Italy), for their facilities to access samples and perform characterization. The scientific support in the etsfmi group, especially Elena Molteni and Guido Fratesi are acknowledged.

Funding The authors have not disclosed any funding.

Declarations

Conflict of interest The authors declare no conflict of interest.

References

Arab, A., Ziari, F., Fazli, M.: Electronic structure and reactivity of (TiO2)n (n=1–10) nano-clusters: Global and local hardness based DFT study. Comput. Mater. Sci. **117**, 90–97 (2016). https://doi.org/10.1016/j.commatsci.2016.01.031

Barborini, E., Piseri, P., Milani, P.: A pulsed microplasma source of high intensity supersonic carbon cluster beams. J. Phys. D Appl. Phys. **32**, L105–L109 (1999). https://doi.org/10.1088/0022-3727/32/21/102

Bukowski, B., Deskins, N.A.: The interactions between TiO2 and graphene with surface inhomogeneity determined using density functional theory. Phys. Chem. Chem. Phys. **17**, 29734–29746 (2015). https://doi.org/10.1039/C5CP04073F

Cao, F., 曹飞, Tan, K., 谭凯, Lin, M.-H., 林梦海, Zhang, Q.-E., 张乾二: A density functional study of N-doped TiO2 anatase cluster. (2021)

Chiodi, M., Cheney, C.P., Vilmercati, P., Cavaliere, E., Mannella, N., Weitering, H.H., Gavioli, L.: Enhanced dopant solubility and visible-light absorption in Cr–N codoped TiO2 nanoclusters. J. Phys. Chem. C **116**, 311–318 (2012). https://doi.org/10.1021/jp208834n

Della Foglia, F., Losco, T., Piseri, P., Milani, P., Selli, E.: Photocatalytic activity of nanostructured TiO_2 films produced by supersonic cluster beam deposition. J. Nanopart. Res. **11**, 1339–1348 (2009). https://doi.org/10.1007/s11051-009-9691-1

Di Liberto, G., Tosoni, S., Pacchioni, G.: Nitrogen doping in coexposed (001)–(101) anatase TiO_2 surfaces: a DFT study. Phys. Chem. Chem. Phys. **21**, 21497–21505 (2019). https://doi.org/10.1039/C9CP03930A

Di Valentin, C., Finazzi, E., Pacchioni, G., Selloni, A., Livraghi, S., Paganini, M.C., Giamello, E.: N-doped TiO_2: theory and experiment. Chem. Phys. **339**, 44–56 (2007). https://doi.org/10.1016/j.chemphys.2007.07.020

Drabik, M., Choukourov, A., Artemenko, A., Polonskyi, O., Kylian, O., Kousal, J., Nichtova, L., Cimrova, V., Slavinska, D., Biederman, H.: Structure and composition of titanium nanocluster films prepared by a gas aggregation cluster source. J. Phys. Chem. C **115**, 20937–20944 (2011). https://doi.org/10.1021/jp2059485

Frisch, M.J., Trucks, G.W., Schlegel, H.B., Scuseria, G.E., Robb, M.A., Cheeseman, J.R., Scalmani, G., Barone, V., Petersson, G.A., Nakatsuji, H.: Gaussian 16, Revision C. 01. Gaussian, Inc., Wallingford CT. 2016. Google Scholar There is no corresponding record for this reference. (2020)

Fronzi, M., Iwaszuk, A., Lucid, A., Nolan, M.: Metal oxide nanocluster-modified TiO2 as solar activated photocatalyst materials. J. Phys. Condens. Matter Inst. Phys. J. **28**, 74006 (2016). https://doi.org/10.1088/0953-8984/28/7/074006

Ghuman, K.K., Goyal, N., Prakash, S.: Vibrational density of states of TiO_2 nanoparticles. J. Non Cryst. Solids **373–374**, 28–33 (2013). https://doi.org/10.1016/j.jnoncrysol.2013.04.022

Giannozzi, P., Baroni, S., Bonini, N., Calandra, M., Car, R., Cavazzoni, C., Ceresoli, D., Chiarotti, G.L., Cococcioni, M., Dabo, I., Dal Corso, A., de Gironcoli, S., Fabris, S., Fratesi, G., Gebauer, R., Gerstmann, U., Gougoussis, C., Kokalj, A., Lazzeri, M., Martin-Samos, L., Marzari, N., Mauri, F., Mazzarello, R., Paolini, S., Pasquarello, A., Paulatto, L., Sbraccia, C., Scandolo, S., Sclauzero, G., Seitsonen, A.P., Smogunov, A., Umari, P., Wentzcovitch, R.M.: QUANTUM ESPRESSO: a modular and open-source software project for quantum simulations of materials. J. Phys. Condens. Matter **21**, 395502 (2009). https://doi.org/10.1088/0953-8984/21/39/395502

Gnanasekaran, L., Hemamalini, R., Ravichandran, K.: Synthesis and characterization of TiO_2 quantum dots for photocatalytic application. J. Saudi Chem. Soc. **19**, 589–594 (2015). https://doi.org/10.1016/j.jscs.2015.05.002

Gui, Y., Liu, D., Li, X., Tang, C., Zhou, Q.: DFT-based study on H_2S and SOF_2 adsorption on Si-MoS_2 monolayer. Results Phys. **13**, 102225 (2019). https://doi.org/10.1016/j.rinp.2019.102225

Javed, S., Islam, M., Mujahid, M.: Synthesis and characterization of TiO_2 quantum dots by sol gel reflux condensation method. Ceram. Int. **45**, 2676–2679 (2019). https://doi.org/10.1016/j.ceramint.2018.10.163

Jia, T., Fu, F., Yu, D., Cao, J., Sun, G.: Facile synthesis and characterization of N-doped TiO_2/C nanocomposites with enhanced visible-light photocatalytic performance. Appl. Surf. Sci. **430**, 438–447 (2018). https://doi.org/10.1016/j.apsusc.2017.07.024

Kakil, S.A., Abdullah, H.Y., Abdullah, T.G.: Electronic properties of (TiO_2)33 nanocrystals with nitrogen impurities at different facets: a DFT study. Mol. Simul. **47**, 1185–1197 (2021). https://doi.org/10.1080/08927022.2021.1962010

Kakil, S.A., Abdullah, H.Y., Abdullah, T.G., Manini, N.: Subsurface depth dependence of nitrogen doping in TiO_2 anatase: a DFT study. J. Phys. Condens. Matter. **33**, 205703 (2021). https://doi.org/10.1088/1361-648X/abce41

Karkare, M.M.: Estimation of band gap and particle size of TiO2 nanoparticle synthesized using sol gel technique. In: 2014 International Conference on Advances in Communication and Computing Technologies (ICACACT 2014). pp. 1–5 (2014)

Kresse, G., Joubert, D.: From ultrasoft pseudopotentials to the projector augmented-wave method. Phys. Rev. B **59**, 1758–1775 (1999). https://doi.org/10.1103/PhysRevB.59.1758

Lamiel-Garcia, O., Cuko, A., Calatayud, M., Illas, F., Bromley, S.T.: Predicting size-dependent emergence of crystallinity in nanomaterials: titania nanoclusters versus nanocrystals. Nanoscale **9**, 1049–1058 (2017). https://doi.org/10.1039/C6NR05788H

Lee, C., Yang, W., Parr, R.G.: Development of the Colle-Salvetti correlation-energy formula into a functional of the electron density. Phys. Rev. B Condens. Matter. **37**, 785–789 (1988). https://doi.org/10.1103/physrevb.37.785

Lin, H., Huang, C.P., Li, W., Ni, C., Shah, S.I., Tseng, Y.-H.: Size dependency of nanocrystalline TiO_2 on its optical property and photocatalytic reactivity exemplified by 2-chlorophenol. Appl. Catal. B Environ. **68**, 1–11 (2006). https://doi.org/10.1016/j.apcatb.2006.07.018

Lundqvist, M.J., Nilsing, M., Persson, P., Lunell, S.: DFT study of bare and dye-sensitized TiO_2 clusters and nanocrystals. Int. J. Quantum Chem. **106**, 3214–3234 (2006). https://doi.org/10.1002/qua.21088

Madhusudan Reddy, K., Manorama, S.V., Ramachandra Reddy, A.: Bandgap studies on anatase titanium dioxide nanoparticles. Mater. Chem. Phys. **78**, 239–245 (2003). https://doi.org/10.1016/S0254-0584(02)00343-7

Mahmoud, Z.H., Adham AL-Bayati, R., Khadom, A.A.: Modified anatase phase of TiO_2 by WO_3 nanoparticles: structural, morphology and spectral evaluations. Mater. Today Proceed. **69**, 799–804 (2021). https://doi.org/10.1016/j.matpr.2021.09.040

Majid, A., Bibi, M.: First principles study of vibrational dynamics of ceria-titania hybrid clusters. J. Nanopart. Res. **19**, 122 (2017). https://doi.org/10.1007/s11051-017-3823-9

Mandal, S., Jain, N., Pandey, M.K., Sreejakumari, S.S., Shukla, P., Chanda, A., Som, S., Das, S., Singh, J.: Ultra-bright emission from Sr doped TiO(2) nanoparticles through r-GO conjugation. R. Soc. Open Sci. **6**, 190100 (2019). https://doi.org/10.1098/rsos.190100

Milani, P., Piseri, P., Barborini, E., Podesta, A., Lenardi, C.: Cluster beam synthesis of nanostructured thin films. J. Vac. Sci. Technol, A **19**, 2025–2033 (2001). https://doi.org/10.1116/1.1331289

Monticone, S., Tufeu, R., Kanaev, A.V., Scolan, E., Sanchez, C.: Quantum size effect in TiO_2 nanoparticles: does it exist? Appl. Surf. Sci. **162–163**, 565–570 (2000). https://doi.org/10.1016/S0169-4332(00)00251-8

Ogata, S., Iyetomi, H., Tsuruta, K., Shimojo, F., Kalia, R.K., Nakano, A., Vashishta, P.: Variable-charge interatomic potentials for molecular-dynamics simulations of TiO_2. J. Appl. Phys. **86**, 3036–3041 (1999). https://doi.org/10.1063/1.371165

Ohsaka, T.: Temperature dependence of the raman spectrum in anatase TiO_2. J. Phys. Soc. Jpn. **48**, 1661–1668 (1980). https://doi.org/10.1143/JPSJ.48.1661

Oprea, C.I., Gîrțu, M.A.: Structure and electronic properties of TiO_2 nanoclusters and dye-nanocluster systems appropriate to model hybrid photovoltaic or photocatalytic applications. Nanomaterials **3**, 357 (2019)

Persson, P., Bergström, R., Lunell, S.: Quantum chemical study of photoinjection processes in dye-sensitized TiO_2 nanoparticles. J. Phys. Chem. B **104**, 10348–10351 (2000). https://doi.org/10.1021/jp002550p

Piseri, P., Li Bassi, A., Milani, P.: Time-of-flight analysis of neutral cluster beams through detection of charged particles produced by cluster impact on a channeltron. Rev. Sci. Instrum. **69**, 1647–1649 (1998). https://doi.org/10.1063/1.1148869

Qu, Z., Kroes, G.-J.: Theoretical study of the electronic structure and stability of titanium dioxide clusters (TiO2)n with n = 1–9. J. Phys. Chem. B **110**, 8998–9007 (2006). https://doi.org/10.1021/jp056607p

Salazar-Villanueva, M., Hernandez, A.B., Anota, E.C., Valdez, S., Cuchillo, O.V.: Electronic and structural properties of Ti9XO20 (X = Ti, C, si, Ge, Sn and pb) clusters: A DFT study. Phys. E Low Dimens. Syst. Nanostruct. **65**, 120–124 (2015). https://doi.org/10.1016/j.physe.2014.09.009

Selli, D., Fazio, G., Valentin, C.: Using density functional theory to model realistic TiO_2 nanoparticles, their photoactivation and interaction with water. Catalysts **7**, 357 (2017). https://doi.org/10.3390/catal7120357

Shyjumon, I., Gopinadhan, M., Helm, C.A., Smirnov, B.M., Hippler, R.: Deposition of titanium/titanium oxide clusters produced by magnetron sputtering. Thin Solid Films **500**, 41–51 (2006). https://doi.org/10.1016/j.tsf.2005.11.006

Srivastava, S., Thomas, J.P., Rahman, M.A., Abd-Ellah, M., Mohapatra, M., Pradhan, D., Heinig, N.F., Leung, K.T.: Size-selected TiO_2 nanocluster catalysts for efficient photoelectrochemical water splitting. ACS Nano **8**, 11891–11898 (2014). https://doi.org/10.1021/nn505705a

Valero, R., Morales-García, Á., Illas, F.: Theoretical modeling of electronic excitations of gas-phase and solvated TiO_2 nanoclusters and nanoparticles of interest in photocatalysis. J. Chem. Theory Comput. **14**, 4391–4404 (2018). https://doi.org/10.1021/acs.jctc.8b00651

Xu, C.Y., Zhang, P.X., Yan, L.: Blue shift of Raman peak from coated TiO_2 nanoparticles. J. Raman Spectrosc. **32**, 862–865 (2001). https://doi.org/10.1002/jrs.773

Zhang, H., Chen, B., Banfield, J.F., Waychunas, G.A.: Atomic structure of nanometer-sized amorphous TiO_2. Phys. Rev. B **78**, 214106 (2008). https://doi.org/10.1103/PhysRevB.78.214106

Zhao, Y., Li, C., Liu, X., Gu, F., Jiang, H., Shao, W., Zhang, L., He, Y.: Synthesis and optical properties of TiO_2 nanoparticles. Mater. Lett. **61**, 79–83 (2007). https://doi.org/10.1016/j.matlet.2006.04.010